



# Cenozoic rejuvenation events of Massif Central topography (France): Insights from cosmogenic denudation rates and river profiles



Valerio Olivetti\*, Vincent Godard, Olivier Bellier, ASTER Team<sup>1</sup>

Aix-Marseille Université (AMU), IRD, CNRS, CEREGE UM34, BP 80, 13545 Aix-en-Provence Cedex 4, France

## ARTICLE INFO

### Article history:

Received 8 October 2015  
Received in revised form 29 March 2016  
Accepted 30 March 2016  
Available online xxxx  
Editor: A. Yin

### Keywords:

<sup>10</sup>Be cosmogenic nuclides  
denudation rates  
river longitudinal profiles  
French Massif Central

## ABSTRACT

The French Massif Central is a part of the Hercynian orogenic belt that currently exhibits anomalously high topography. The Alpine orogenesis, which deeply marked Western European topography, involved only marginally the Massif Central, where Cenozoic faulting and short-wavelength crustal deformation is limited to the Oligocene rifting. For this reason the French Massif Central is a key site to study short- and long-term topographic response in a framework of slow tectonic activity. In particular the origin of the Massif Central topography is a topical issue still debated, where the role of mantle upwelling is invoked by different authors. Here we present a landscape analysis using denudation rates derived from basin-averaged cosmogenic nuclide concentrations coupled with longitudinal river profile analysis. This analysis allows us to recognize that the topography of the French Massif Central is not fully equilibrated with the present base level and in transient state.

Our data highlight the coexistence of out-of-equilibrium river profiles, incised valleys, and low cosmogenically derived denudation rates ranging between 40 mm/kyr and 80 mm/kyr. Addressing this apparent inconsistency requires investigating the parameters that may govern erosion processes under conditions of reduced active tectonics. The spatial distribution of denudation rates coupled with topography analysis enabled us to trace the signal of the long-term uplift history and to propose a chronology for the uplift evolution of the French Massif Central.

© 2016 Elsevier B.V. All rights reserved.

## 1. Introduction

Located in the foreland domain of both the Alpine and Pyrenean mountain belts, the intracontinental French Massif Central presents intriguing topographic features that have been the aim of decades of geological studies. The origin and timing of topography development are still debated. While the orogenic phase and faulting is mainly Hercynian, the present topography of the French Massif Central is remarkably higher than other Hercynian belt remnants. Moreover, the moderately elevated topography, that reaches 1700 m a.s.l., did not originate from Alpine compressional tectonic regime, or from extensional tectonics. In fact, during Mesozoic and Cenozoic, the Massif Central was involved only marginally in the main tectonic events that strongly modified the topography of the Africa–Europe plate boundary (Dewey et al., 1989). The nearly undeformed Mesozoic sedimentary cover (Séranne et al., 2002) as well as Mesozoic low-temperature thermochronological ages (i.e.

Peyaud et al., 2005; Gautheron et al., 2009) indicate that Cenozoic crustal deformation and million-year-timescale denudation have been very limited. For this reason the French Massif Central is a key site to study the intriguing issue of coexistence of high topography and slow deformation in ancient mountain ranges, and to discriminate whether the present topography simply reflects the post-orogenic isostatic compensation or a recent pulse of uplift (e.g. Baldwin et al., 2003; Tucker and van der Beek, 2013).

Recently, numerous studies have focused on landscape evolution in a context of limited crustal deformation such as the Appalachian range (Miller et al., 2013; Dethier et al., 2014), west Indian margin (Mandal et al., 2015), or the eastern Tibetan plateau (Ansberque et al., 2015). In fact, regions of limited fault activity are considered ideal to study the coherence between landscape morphology and denudation rates. Faulting induces local crustal block movements pushing the landscape toward transient conditions which prevent to extract regional constraints on tectonic evolution (Whipple and Tucker, 1999; Kirby and Whipple, 2012). Coupling between uplift rates and cosmogenically derived denudation rates have been recently recognized in a variety of landscapes undergoing different rates of tectonic uplift, in high uplift mountain ranges such as the Northern and Southern Apennines (Cyr et al., 2010),

\* Corresponding author at: Technopôle Environnement Arbois – Méditerranée, BP 80, 13545 Aix en Provence Cedex 4, France.

E-mail address: [olivetti@cerge.fr](mailto:olivetti@cerge.fr) (V. Olivetti).

<sup>1</sup> Maurice Arnold, Georges Aumaitre, Didier L. Bourlès, Karim Keddadouche.

San Gabriel Mountains (DiBiase et al., 2010), Eastern Alps (Legrain et al., 2015) as well as in regions experiencing slow uplift rates (Matmon et al., 2003; Meyer et al., 2010). Along profile changes in denudation rates generally indicate a landscape that is transiently responding to modified external conditions (i.e. Kirby and Whipple, 2012). In this framework, transient landscapes become a useful tool to investigate the timing and intensity of the associated tectonic changes.

Here, we use denudation rates derived from basin-averaged cosmogenic nuclide concentrations (hereafter: cosmogenic denudation rates) and longitudinal river profiles to investigate landscape evolution in the eastern Massif Central. Millennial-timescale cosmogenic denudation rates are compared with catchment slope and morphometric river indices to quantify the present morphological evolution and its spatial pattern. River long profiles are used to study the relationship between tectonic forcing, incision and landscape response over a longer time scale ( $10^3$  to  $10^6$  yr). This analysis allows addressing several key questions with respect to landscape evolution: how old is the topography of the Massif Central? Does the topography record tectonic uplift? What are the main factors controlling denudation rates?

Our results highlight that the topography of the eastern French Massif Central is currently in a transient state. The denudation rates show a spatial pattern reflecting the coexistence of modern and ancient landscapes, which is confirmed by out-of-equilibrium river profiles and distinct relict landscapes. On the basis of these observations, we propose that the landscape evolved through two main phases: a Paleogene to Neogene uplift event that generated the main topography and recent rejuvenation triggered by post-Pliocene regional uplift.

## 2. Study area

The French Massif Central is located directly west of the Alpine belt, across the Rhône river valley, and presents a roughly triangular shape in plan view, with sides  $\sim 350$  km long (Fig. 1). The topography is characterized by a low-relief high-elevation surface reaching 1700 m above sea level and gentle marginal flanks, except for the southeastern margin, which is controlled by the northeast directed Cevenne fault system (Séranne et al., 2002). On the eastern side, the massif is bounded by a steep erosive escarpment formed by the Rhône river. The drainage divide separating rivers draining towards the Atlantic from those draining to the Mediterranean runs close to the southeastern and eastern margins, which correspond to some of the highest elevations of the massif. This results in an asymmetric topography with a steeper SE margin (swath profiles A and B of Fig. 1). The highest elevations coincide with Cenozoic volcanic edifices, but large portions of the crystalline basement have comparable elevations (Fig. 1). To analyze the long wavelength topographic signal and isolate regional scale features, we filtered the topography at 10 km and 50 km wavelengths (Fig. 1). The asymmetric topography is evident also in the 50 km filtered topography while other topographic features tend to vanish, such as the Limagne and Roanne basins in the northern study area.

The tectonic evolution of the French Massif Central extends back to the Late Paleozoic, when the Hercynian orogeny induced the growth and decay of a highly elevated mountain belt (i.e. Peyaud et al., 2005; Blés et al., 1989). The lithology outcropping in the studied area is dominated by the Hercynian crystalline basement with mostly plutonic and high-grade metamorphic rocks. Mesozoic–Cenozoic sedimentary rocks, mainly limestones, unconformably cover the borders of the massif, except along the eastern flank where the study area of this work is located. A NE-trending strike-slip fault system is associated with an E–W directed compressional episode late Carboniferous in age (Blés et al., 1989).

Along the southern margin of the Massif Central, the NE–SW striking fault system has been reactivated during the Mesozoic to the Cenozoic, mainly during Oligocene rifting and opening of the Gulf of Lion (Merle et al., 1998; Blés et al., 1989). In the northern Massif Central, Oligocene rifting produced N-trending normal faults that controlled the opening of N–S elongated basins such as the Limagne, Roanne and Bresse grabens (Fig. 1) (Merle et al., 1998). During the Cenozoic, the Massif Central was only marginally involved in the Pyrenean and Alpine tectonic phases, which strongly deformed the sedimentary basins surrounding the massif to the south and east. Although the Alpine frontal thrusts are only a few tens of kilometers to the East, no evidence of Alpine deformation is reported within the crystalline basement of the massif (Blés et al., 1989).

Over the last 50 years, the seismic activity of the Massif Central, revealed by a dozen of  $M_w$  3.5 events, is focused beneath the Limagne basin at its northern margin, while the rest of the massif recorded extremely limited instrumental seismicity (Mazabraud et al., 2005).

In contrast with the limited crustal deformation, volcanism has been the first-order process contributing to topographic modifications of the Massif Central during the Cenozoic. A first volcanic phase began during the Paleocene, and a second one occurred during Oligocene rifting, while the largest emplacement of volcanic deposits took place since the middle Miocene (15 Ma) and is not related with any rifting phase (Michon and Merle, 2001). The negative Bouguer anomalies, the high heat flow and a low P-wave velocity anomaly indicate the presence of hot material at upper mantle depths, suggesting that mantle upwelling may contribute to the volcanism (i.e. Barruol and Granet, 2002). Several authors proposed that volcanism could be linked to a regional uplift; for instance, Michon and Merle (2001) correlate the two Miocene peaks of volcanism with two uplift phases induced by thermal erosion at the base of the lithosphere, while others invoke an uplift that is dynamically sustained by mantle flow (Barruol and Granet, 2002; Faccenna et al., 2010).

## 3. Methods

### 3.1. Topographic analysis and knickpoint identification

We used a digital elevation model (DEM) released by the IGN (French Institut Géographique National, BD ALTI<sup>®</sup> product) with a pixel resolution of 50 m to extract topographic metrics from each of the sampled catchments and rivers, such as mean slope, longitudinal profiles, concavity and steepness indices. River longitudinal profiles can be described by an empirical power law relating local channel slope and drainage area, taken as a proxy for discharge (e.g. Whipple and Tucker, 1999; Kirby and Whipple, 2012):  $S = k_s A^{-\theta}$  where  $S$  is the local channel slope,  $A$  is the upstream contributing drainage area, and  $k_s$  and  $\theta$  are morphological indices known as the steepness index and concavity index, respectively.  $S$  and  $A$  are easily extracted from DEM and plotted in a log–log plot to infer  $k_s$  and  $\theta$  from regression.

In steady state and for uniform lithology,  $k_s$  is theoretically and empirically validated to vary systematically with the rate of rock uplift (i.e. Kirby and Whipple, 2012). In the absence of rock uplift, the steepness index declines through time, with a rate controlled by the erodibility properties of the bedrock (Whipple, 2004). In many cases, the river profile presents a non-regular concave-up form that is characterized by segments with regular slope separated by knickpoints. Depending on their origin, knickpoints can exhibit contrasting characteristic (Whipple, 2004). Equilibrium knickpoints, such as those related to lithologies with differing erodibility, tend to be stable and separate two segments with similar concavity index; disequilibrium knickpoints, such as

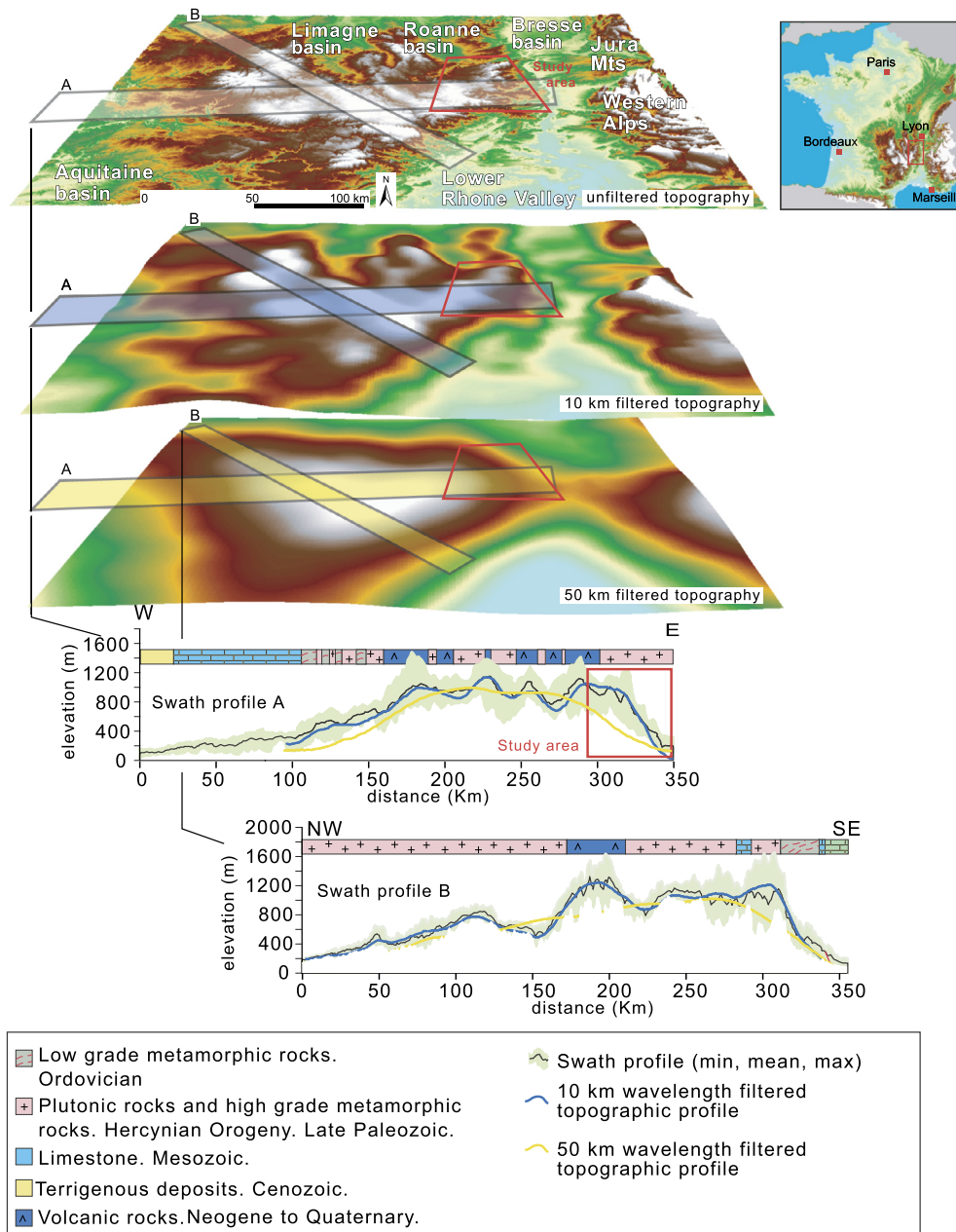


**Fig. 1.** Topographic features of the French Massif Central. (a) Topography from a Digital Elevation Model (DEM) with a pixel resolution of 50 m (IGN BD ALTI®). (b) Filtered topography at 10 km and (c) 50 km wavelengths. The locations of two swath profiles are indicated by rectangles. (d) Maximum, minimum and mean topography along the two profiles. In each profile, blue and yellow lines correspond to the 10 and 50 km filtered topography, respectively. (For interpretation of the references to color in this figure legend, the reader is referred to the web version of this article.)

those related to temporal change in uplift rate, migrate faster and separate two segments characterized by different concavity indices (Kirby and Whipple, 2012; Wobus et al., 2006).

In this study, we conducted morphometric analysis using ArcGIS to generate the hydrographic network and MATLAB scripts (download from: [geomorphptools.org](http://geomorphptools.org)) (Snyder et al., 2000; Wobus et al., 2006) to extract and analyze river profiles and to generate log–log area–slope diagrams used to calculate steepness and concavity indices.

### 3.2. Cosmogenic denudation rates

We determined catchment-averaged denudation rates from the concentrations of cosmogenic beryllium-10 ( $^{10}\text{Be}$ ) in quartz-bearing modern river sand.  $^{10}\text{Be}$  accumulates in quartz grains near

the Earth's surface proportionally to its local production rate (corrected for latitude and elevation) and inversely proportionally to the surface denudation rate (i.e. von Blanckenburg, 2005). To minimize the effects of lithologic differences on denudation rates, we sampled catchments draining rock with uniform quartz content and similar response to denudation, such as granite and high grade metamorphic rocks. Samples were collected from either side of the drainage divide, from catchments draining both toward the Atlantic Ocean and the Mediterranean Sea. The majority of samples were collected upstream of knickpoints. River sand samples were collected from freshly exposed sandy bars of active channels in 27 catchments, with upstream areas between 8 and 600 km<sup>2</sup> (Table 1).

The sand samples were sieved to extract the 250–1000  $\mu\text{m}$  fraction. Magnetic fractions were removed, after which successive

**Table 1**  
Cosmogenic nuclide data.

Sample name	Lon. (°E)	Lat. (°N)	Area <sup>a</sup> (km <sup>2</sup> )	Elevation <sup>b</sup> (m)	Slope (°)	qtz mass <sup>c</sup> (g)	[ <sup>10</sup> Be] 10 <sup>3</sup> (at/g) quartz	Production rate <sup>d</sup> (at/g/yr)	Erosion rate (mm/kyr)	Integration time <sup>e</sup> (yr)
VO-01	4.7272	45.4133	37.57	631	12.5	10.84	161.42 ± 6.55	7.62 ± 3.22	40.09 ± 3.17	14966
VO-02	4.7402	45.3852	26.19	478	8.3	8.97	149.18 ± 5.50	6.67 ± 3.04	39.04 ± 2.98	15369
VO-03	4.6827	45.3461	19.96	565	9.1	10.21	174.73 ± 5.91	7.20 ± 2.71	35.19 ± 2.67	17050
VO-04	4.5558	45.3014	28.28	1018	13.4	11.02	184.17 ± 7.91	10.50 ± 3.82	45.84 ± 3.77	13089
VO-05	4.5497	45.2875	36.77	969	14.0	10.64	184.35 ± 5.91	10.08 ± 3.44	44.23 ± 3.39	13565
VO-06	4.4078	45.2386	24.2	1074	7.2	10.84	253.47 ± 8.03	10.98 ± 2.70	34.25 ± 2.67	17518
VO-07	4.4119	45.2364	8.76	1039	10.2	10.78	186.8 ± 6.14	10.66 ± 3.59	45.77 ± 3.54	13109
VO-08	4.3806	45.2089	67.05	1060	9.3	10.14	188.09 ± 6.38	10.84 ± 3.64	46.1 ± 3.59	13015
VO-09	4.2942	45.1414	20.41	1000	4.6	10.48	214.04 ± 6.84	10.32 ± 3.03	38.69 ± 2.99	15508
VO-10	4.3042	45.1072	13.58	1022	6.1	9.35	214.81 ± 6.87	10.50 ± 3.07	39.13 ± 3.02	15334
VO-11	4.5014	45.1739	18.13	993	18.2	10.59	106.17 ± 3.63	10.27 ± 6.16	79.18 ± 6.03	7578
VO-12	4.6394	45.2353	114.08	828	16.2	9.79	153.05 ± 5.00	8.97 ± 3.74	48.58 ± 3.68	12351
VO-13	4.7761	45.2536	15.99	379	4.2	9.98	82.99 ± 3.70	6.10 ± 5.38	67.33 ± 5.27	8911
VO-14	4.7606	45.2350	7.95	377	2.9	10.68	121.06 ± 4.63	6.09 ± 3.50	45.25 ± 3.44	13260
VO-15	4.8038	45.1424	33.79	424	5.7	10.48	127.09 ± 9.73	6.35 ± 4.62	44.46 ± 4.58	13495
VO-16	4.5961	45.1400	16.1	860	16.0	10.70	159.95 ± 8.89	9.21 ± 4.27	47.45 ± 4.22	12645
VO-17	4.8057	44.9002	15.19	448	15.5	9.26	146.51 ± 9.76	6.47 ± 3.75	38.85 ± 3.72	15444
VO-18	4.6657	44.9560	10.72	736	4.9	10.04	197.21 ± 9.16	8.28 ± 2.95	34.92 ± 2.92	17182
VO-19	4.5291	44.9928	192.46	876	14.4	9.99	113.14 ± 8.36	9.31 ± 7.00	68.42 ± 6.92	8769
VO-20	4.3922	45.0192	11.38	1080	3.5	9.99	211.93 ± 10.37	10.99 ± 3.60	41.28 ± 3.56	14535
VO-21	4.5017	45.0431	118.14	936	14.5	10.02	121.45 ± 8.84	9.78 ± 6.75	66.3 ± 6.67	9050
VO-22	4.2108	45.2168	232.73	951	7.5	10.02	153.2 ± 9.22	9.93 ± 4.93	52.85 ± 4.87	11353
VO-23	4.6627	45.0733	62.15	712	14.1	10.91	146.71 ± 9.62	8.13 ± 4.50	46.79 ± 4.46	12823
VO-24	4.7238	45.0579	377.04	739	13.3	10.00	110.48 ± 8.29	8.32 ± 6.57	63.94 ± 6.5	9384
VO-25	4.7804	45.0644	618.91	667	12.2	10.04	112.42 ± 8.88	7.83 ± 6.32	59.78 ± 6.26	10037
VO-26	4.7561	45.0111	70.97	551	8.2	10.01	135.47 ± 8.94	7.08 ± 4.36	45.4 ± 4.31	13216
VO-27	4.8008	44.8560	16.23	491	11.7	9.50	79.3 ± 8.43	6.71 ± 9.74	76 ± 9.66	7895

<sup>a</sup> Basin mean elevation from 50 m DEM.

<sup>b</sup> Catchment mean slope calculated from 50 m DEM.

<sup>c</sup> Mass of pure quartz dissolved.

<sup>d</sup> Spallation production rate scaling factor according to Stone (2000).

<sup>e</sup> Timescale of integration for denudation ( $T = z^*/\text{denudation rate}$ , with  $z^*$  the absorption depth scale). Four procedural blanks have been processed. Their associated <sup>10</sup>Be/<sup>9</sup>Be ratios are:  $2.25 \pm 0.37 \times 10^{-15}$ ,  $3.4 \pm 0.48 \times 10^{-15}$ ,  $1.78 \pm 0.39 \times 10^{-15}$ ,  $1.47 \pm 0.49 \times 10^{-15}$ , which is at least one order of magnitude lower than those associated with the processed samples. Uncertainties on <sup>10</sup>Be concentrations include: an external machine uncertainty (0.5%), a certified standard ratio uncertainty (1.08%), the mean of the standard ratio measurements ( $1\sigma$ ), a statistical error on counted <sup>10</sup>Be events ( $1\sigma$ ), and the uncertainty associated with the chemical and analytical blank correction. An external uncertainty of 10% was affected to the production rate calculation and was included in the total uncertainties on denudation rate.

leachings with a one-third (by volume) HCl solution and two-thirds (by volume) H<sub>2</sub>SiF<sub>6</sub> solution were applied until pure quartz was obtained (Merchel et al., 2008). Three additional HF leachings were used to remove atmospheric <sup>10</sup>Be present on quartz grains. The samples were spiked with 100 μL of an in-house <sup>9</sup>Be carrier solution ( $3.03 \cdot 10^{-3} \text{ g g}^{-1}$ ) before total digestion. Beryllium was finally extracted using standard ion exchange columns and oxidized into BeO. The <sup>10</sup>Be/<sup>9</sup>Be ratios were measured by accelerator mass spectrometry (AMS) at the French national facility ASTER. These ratios were calibrated against the National Institute of Standards and Technology standard reference material 4325 with an assigned isotopic ratio of  $2.79 \pm 0.03 \cdot 10^{-11}$  (Nishiizumi et al., 2007) and corrected for procedural blanks.

Measured <sup>10</sup>Be concentrations were converted to catchment-averaged denudation using the CRONUS-Earth online calculator (Balco et al., 2008) version 2.2 (<http://hess.ess.washington.edu/>) based on the time-dependent form of the Lal (1991) scaling model. The reference nucleonic <sup>10</sup>Be production rate for this scaling scheme is  $4.39 \pm 0.37 \text{ atoms g}_{\text{qtz}}^{-1} \text{ yr}^{-1}$  using the revised 07KN-STD standardization (Nishiizumi et al., 2007).

## 4. Results

### 4.1. Channel morphology

Within the study area, 56 rivers have been analyzed to extract longitudinal profiles, steepness index, concavity and knickpoint elevations. Because of different base levels, profile shapes and topographic settings, the rivers of the east-draining (Mediterranean) and west-draining (Atlantic) flanks are described separately. Along the Mediterranean-draining flank, the right-side tributaries of the

Rhône river from St. Etienne to Valence (Fig. 2) include rivers spanning from 5 km to 75 km in stream length. We found 38 knickpoints, which exhibit a mean elevation of 400 m (Fig. 3). The majority ( $n = 30$ , 79%) of the knickpoints lies between 427 m and 273 m a.s.l. and are clustered within 150 m of elevation (Fig. 3b–c). Remaining knickpoints ( $n = 8$ , 21%) are evenly distributed between 463 m and 1059 m a.s.l. A comparison of the knickpoint position with geological maps (BRGM 1:50000 scale) shows that very few of these knickpoints coincide with changes in rock type (Fig. 1 and Fig. S1). However, the lithology varies from granite, migmatite to high-grade metamorphic rocks that are considered to have a similar response to erosion. Therefore we retain that lithologic control on the knickpoint position is very limited.

Knickpoint positions have been manually defined by coupling information from river profiles and slope–area plots. We define knickpoint at the onset (going downstream) of the change in profile shape. We observe that this point usually corresponds to a change in steepness and concavity indices, in the slope–area plot. In the field they are characterized by a gradual narrowing of the valley and an increase in bedrock exposure.

The knickpoints population between 427 m and 273 m elevation divides the channels into two distinct reaches. The upper reaches show a regular concave-up shape with mean concavity index ( $\theta$ ) of  $0.48 \pm 0.07$  and a mean normalized steepness index ( $k_{sn}$ , normalized for  $\theta = 0.45$ ) of  $41.5 \pm 18.5 \text{ m}^{0.9}$ . The observed mean concavity is close to theoretical values calculated for river where regular uplift is compensated by incision (Whipple and Tucker, 1999). The lower reaches show a strongly irregular profile characterized by a convex shape. In the majority of these profiles, the lower reaches consist in a large and diffuse knickzone with nega-

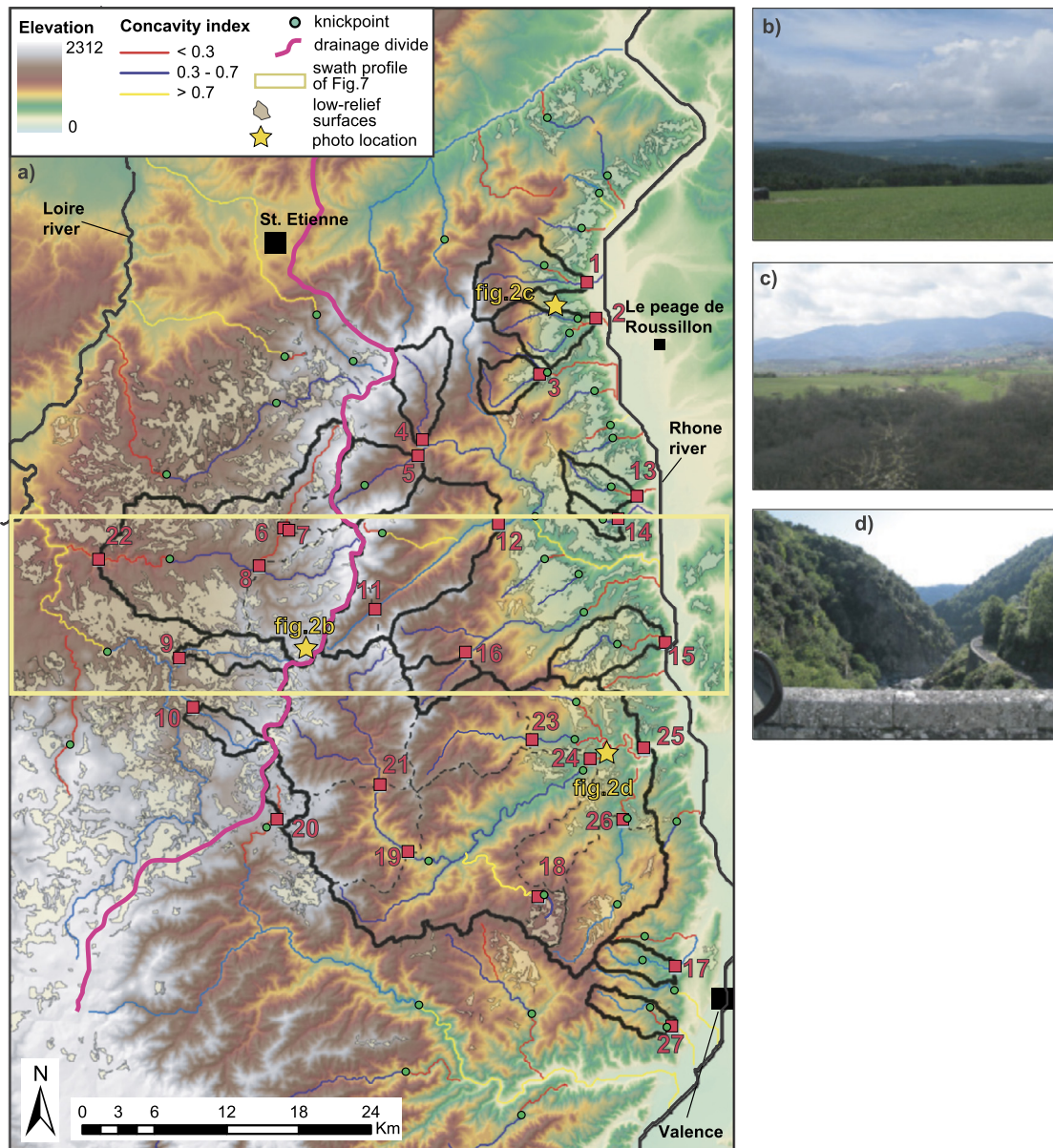


**Fig. 2.** (a) IGN (BD ALTI®) 50 m resolution digital elevation model showing the studied catchments and distribution of best-fit concavity index for the rivers analyzed across the eastern margin of the French Massif Central. Pale blue squares indicate the cosmogenic sampling locations with sample ID used in the main text (Table 1). Thick black lines and dashed black lines are the limits of the main catchments and the sub-catchments respectively. Green circles indicate knickpoints locations. Polygons represent a low slope area ( $<5^\circ$ ) covering crystalline rocks. Yellow stars indicated photo locations. (b) View looking west showing the high-elevation low-relief areas. (c) View looking southwest of the low-elevation low-relief surface developed along the Rhône river. (d) View of a river incision downstream of a knickpoint. (For interpretation of the references to color in this figure legend, the reader is referred to the web version of this article.)

tive concavity index, extending until the present base level of the Rhône.

The western side of the study area drains towards the Loire river and the Atlantic Ocean. We identified a total of 8 knickpoints ranging in elevation between 561 m and 1002 m a.s.l. with an average around 817 m; 5 of them cluster between 717 and 901 m a.s.l. Although western river knickpoints are quite dispersed, they also separate river profiles into distinct segments. Similar to the eastern side, the upper reaches show a regular concave-up shape with a mean concavity of  $0.30 \pm 0.11$  and a mean normalized steepness index of  $35 \pm 10.9 \text{ m}^{0.9}$  (normalized to 0.45 of concavity). Beneath the knickpoint the profiles become steeper and often convex.

In general, for both the western and eastern flanks, the knickpoints seem to separate a regular and concave-up upper reach

from a lower large knickzone, convex in shape and extending to the local base level.

#### 4.2. $^{10}\text{Be}$ -derived denudation rates

Catchment-averaged denudation rates estimated over millennial-timescale from  $^{10}\text{Be}$  concentrations are presented in Fig. 4 and Table 1. The 27 obtained denudation rates range between  $34 \pm 2.7 \text{ mm/kyr}$  and  $79 \pm 6.0 \text{ mm/kyr}$ . They represent 16 catchments and 9 subcatchments, which differ by elevation, mean slope, dimension and side with respect to divide while lithology is uniform across the entire area (Fig. 1). Five of these samples have been collected at the outlet of catchments that exhibit knickpoints and non-equilibrated river profiles. In case of catchments sampled at multiple locations, we calculated the “subcatchment denudation

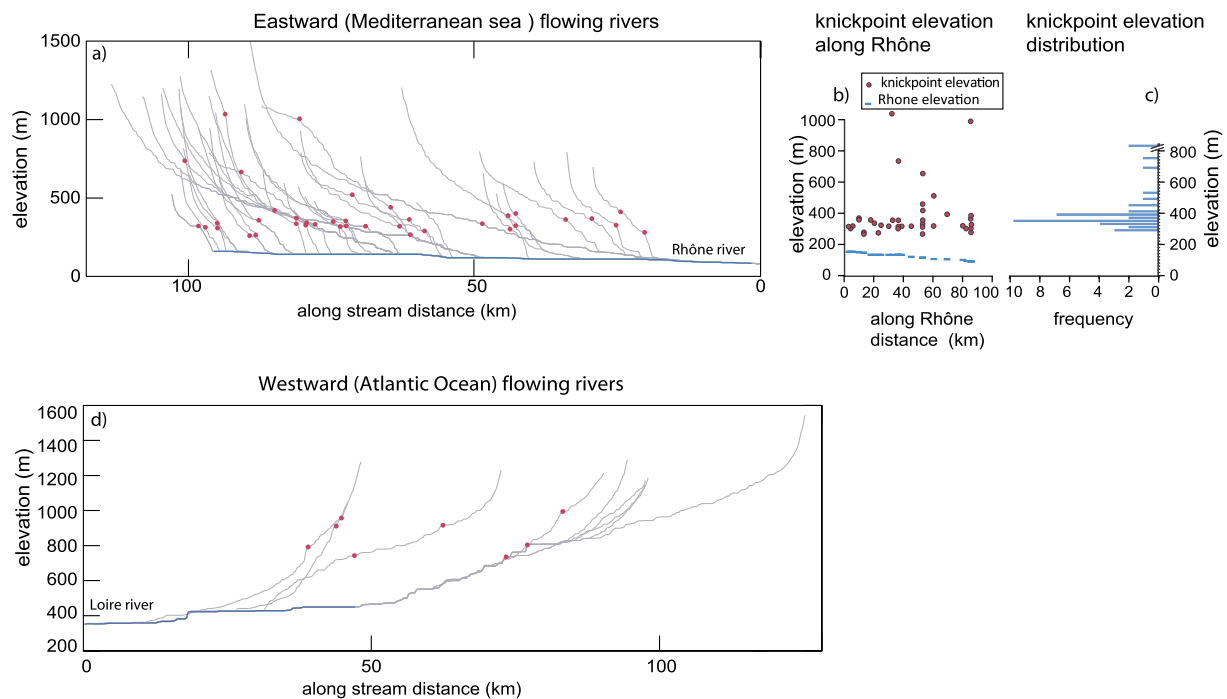


**Fig. 3.** (a) Mediterranean-draining (eastward) longitudinal river profiles of 42 streams showing the location of 38 knickpoints (red circles). (b) Elevation of the eastern flank knickpoints against the distance along the Rhône of the corresponding tributary confluence. Knickpoints with different elevation and same confluence distance are from the same large catchment. (c) Histogram of knickpoint elevations in 20 m bins. (d) Atlantic-draining (westward) longitudinal river profiles of 10 streams showing the location of 8 knickpoints. (For interpretation of the references to color in this figure legend, the reader is referred to the web version of this article.)

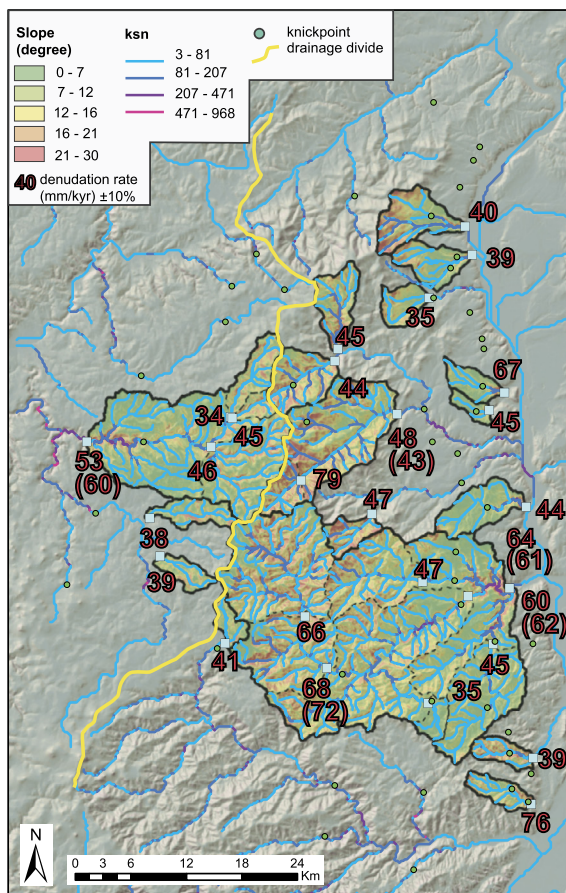


**Fig. 4.** Slope map showing  $^{10}\text{Be}$ -derived denudation rates in mm/kyr. Numbers in brackets indicate deconvolved denudation rates corresponding to relative sub-catchments only (following Granger et al., 1996).

rates”, which is the denudation associated with the area between two successive sampling points (Granger et al., 1996).

The three highest values are associated to catchments draining toward the Mediterranean side, two close to drainage divide (vo11, vo19), and one close to the Rhône confluence (vo27). Moreover, no correlation is observed with elevation or drainage area, which ranges between 10 km<sup>2</sup> and 600 km<sup>2</sup>. At first glance, denudation rates estimated for catchments with knickpoints show values similar to those estimated for catchments that do not contain knickpoints. Overall, the denudation rates in the Massif Central are low and similar to values estimated in ancient orogens such as the Appalachian range (Miller et al., 2013; Matmon et al., 2003), the Laramide belt (Dethier et al., 2014) or Middle Europe (Schaller et al., 2001).

## 5. Data analysis

### 5.1. Low-relief surfaces

The topography of the studied area of the Massif Central shows two low-relief surfaces. Along the east-draining (Mediterranean) flank, between 250 and 400 m a.s.l., a low-relief surface extends between the edge of the present Rhône erosional escarpment to the east, and the foot of the mountain cliff to the west. It runs parallel to the Rhône along the whole studied area. This surface has been previously described by many authors (i.e. Mandier, 1988 and references therein) who interpreted it as a Miocene erosional surface known as the “piedmont Rhodanien”. This surface extends south of the study area, providing a regional feature that marks the entire southern flank of the Massif Central.

Along the west-draining (Atlantic) flank, a high-elevation low-relief (Fig. 2b) surface largely develops between the drainage divide (~1300 m. a.s.l.) and the knickpoint elevation at ~800 m. a.s.l. This high-standing landscape dips gently toward the west and it is characterized by gently incised valleys that separate rolling topography 100–200 m higher than the valley bottoms. Fluvial incision is very

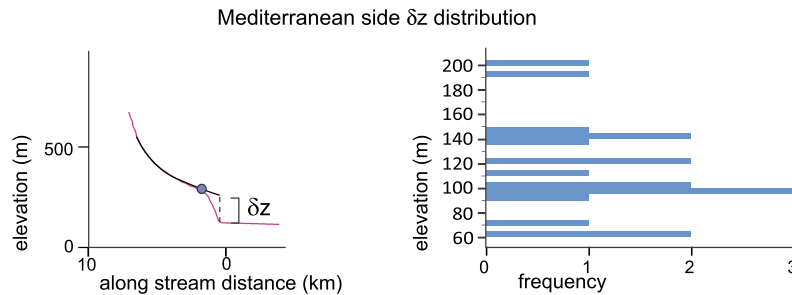


**Fig. 5.** (a) Longitudinal river profile of the River n.2 (Fig. S1) showing the modeled prolongation of the upstream river profile, and the minimum incision ( $\delta z$ ). (b) Histogram of minimum incision values for the Mediterranean-draining streams.

limited and weathering is the dominant processes currently affecting the upland landscape (Wyns and Guillocheau, 1999).

In some catchments, the drainage divide exactly coincides with the limit between the eastern east-draining valleys and the western low relief surface. In other cases, the drainage divide is located within the western low relief surface: in these cases, the eastern catchments encompass a little portion of this low-relief surface (i.e. location of star in Fig. 2b).

### 5.2. Transient landscape analysis

Conventional knowledge holds that the French Massif Central is a mountain belt that has been affected by very low tectonic activity during the Cenozoic (Blés et al., 1989). Therefore, the most striking result of the presented analysis is the evidence for out-of-equilibrium rivers on both the Atlantic and Mediterranean flanks characterized by non-lithologic knickpoints. The analysis of the knickpoints distribution and their relationship with the topography allows investigating their origin.

Considering the 38 knickpoints of the Mediterranean-draining flank, 30 cluster within an elevation range of  $\sim 150$  m (Fig. 4). Theoretical detachment-limited fluvial incision models and experimental numerical modelings predict that all knickpoints have uniform vertical velocity when they originate from a common base level lowering (Niemann et al., 2001). Consequently, we suggest that the majority of the studied knickpoints are genetically linked. In agreement with a knickpoint distribution due to an erosive wave propagating upstream within basins of different sizes (i.e. Wobus et al., 2006), the geographic distribution of these knickpoints (Fig. 3) is dispersed and no alignment trend is evidenced. Comparison with the geological maps and field observations indicates that these knickpoints do not coincide with lithologic contacts or tectonic structures. Moreover, the knickpoint positions do not correspond either to a threshold drainage area between colluvial to alluvial condition.

Downstream of the knickpoints, local relief and hillslope significantly increase with respect to the upper landscape, while the concavity index changes from the value of  $\sim 0.45$ , to low or even negative values. Therefore, the analyzed knickpoints separate two river segments that exhibit very different morphologies: an upper relict landscape not yet involved in the rejuvenation process and a lower strongly disequibrated modern landscape.

Along the eastern flank, the river network shows different patterns below and above knickpoints. Catchments are elongated, narrow, subparallel and without major confluences below the knickpoints. Rivers flow in narrow valleys which locally become canyons (Fig. 2d) with tens of meters high vertical walls cutting through the low relief surface, which extends between 250 and 400 m a.s.l. Knickpoints do not coincide with the Rhône erosional escarpment, and they have retreated upstream in the catchments at distances from the Rhône confluence spanning from a few kilometers up to 10 km. Above the knickpoints, the stream network displays den-

drific drainage patterns, catchments are wider and hillslope angles increase towards the drainage divide. At the divide, the topography is characterized by a high-elevation low-relief surface interpreted as a relict landscape.

In the Mediterranean-draining side, we investigated the relationship between the low-relief surface standing around 400 m, and the present Rhône elevation. We used the river segment above the knickpoint to model the downstream prolongation of the river profile before the knickpoint initiation. This method provides the elevation of the previous relative base level and by comparison with the present base level, it allows to estimate the amount of incision (Kirby and Whipple, 2012). The modeled prolongation of the 18 analyzed rivers leads to a minimum incision of  $120 \pm 40$  m (Fig. 5).

### 5.3. Topography vs denudation rate

The relationships between denudation rates, mean catchment slope and steepness index are presented in Fig. 6. Overall,  $^{10}\text{Be}$ -derived denudation rates and geomorphic parameters do not show significant correlations. Denudation rates are poorly correlated with mean catchment slope ( $R^2 = 0.18$ ) (Fig. 6a), which reaches a maximum value of  $18^\circ$ . Since the first pioneering study focused on erosional topography (i.e. Ahnert, 1970), the nearly linear relationship between mean slope/mean relief and denudation rate has been validated for mean catchment slope lower than  $20^\circ$  (Portenga and Bierman, 2011). Here, we aim to investigate the reasons for this unusually poor correlation.

When the subcatchment denudation rates values are included in the dataset, the correlation coefficient does not change significantly ( $R^2 = 0.12$ ). It is noteworthy that in the two largest catchments (vo-22 and vo-25), the subcatchment denudation rates sampled downstream of the knickpoints are slightly higher than those estimated considering the whole catchment area. This suggests that the contribution of the modern landscape below the knickpoints tends to increase the average denudation rate. To investigate the contribution of the modern landscape to the total denudation, we compare the denudation rates of catchments with knickpoints against the proportion of the catchment located below the knickpoint (Fig. 6c). This comparison indicates that denudation rates are higher when the proportion of modern landscape increases in the catchment.

Better correlation between denudation rates and mean catchment slope is obtained when the 7 values from catchments including knickpoints are removed ( $R^2 = 0.42$ ) (Fig. 6a). Therefore, the poor correlation of the original data could be mainly controlled by the denudation values of the catchments encompassing an incised portion downstream of the knickpoints. Similarly, the relationship between denudation rates and mean normalized steepness index shows poor correlation (Fig. 6b). The mean normalized steepness is calculated over 1 km segment profiles for all rivers upstream of the sampling point (Miller et al., 2013).

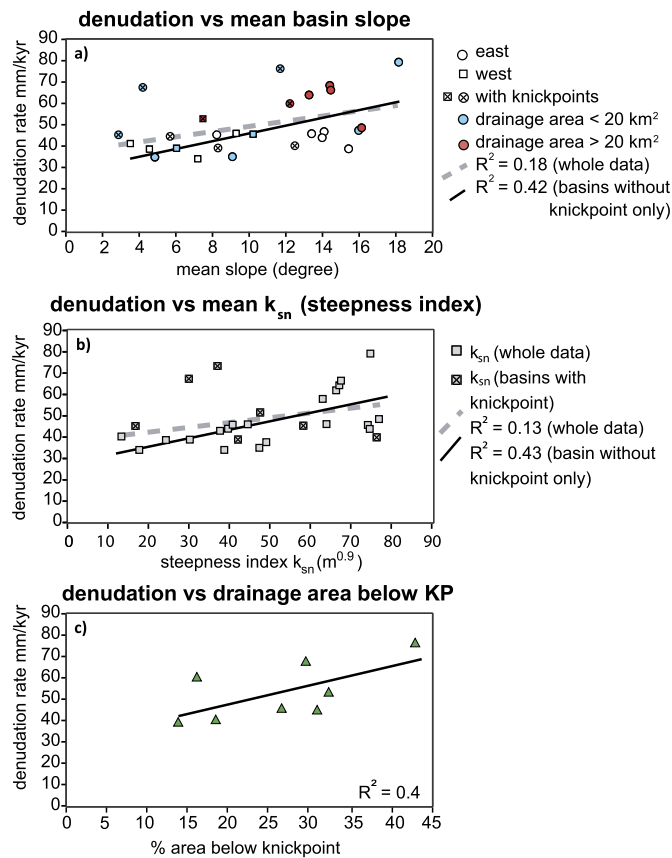


**Fig. 6.** Relationship between topographic parameters and catchment-averaged  $^{10}\text{Be}$ -derived denudation rates. (a) Denudation rates against catchment mean slope. Dotted gray line is the regression of the whole data set, black line is regression of the data concerning the catchment without knickpoint only. (b) Denudation rates against basin-averaged mean normalized steepness index ( $k_{sn}$ ). (c) Denudation rates against the proportion of the catchment located below the knickpoint.

For the catchments sampled downstream of the knickpoints, we studied the correlation of the denudation rate with the mean  $k_{sn}$  extracted both below and above the knickpoints. In both cases, the correlation does not change significantly. When the values of  $k_{sn}$  relative to basins with knickpoints are removed from the dataset, the correlation coefficient increases significantly (Fig. 6b), suggesting again that the values from out of equilibrium catchments are the main reason for the initial poor correlation.

Theoretical formulations predict that denudation rate is correlated to hillslope and river gradient, and its relationship is described by the transport laws that are independent of the fact that landscape is in transient or steady state condition. However, in transient conditions hillslopes may not be equilibrated with river incision and catchments may encompass domains with very contrasted hillslope gradients. A typical example of such decoupling would be the rapid down cutting of a river into a low-relief surface. Rivers may exhibit shallow gradients and the averaged catchment slope may be low, but denudation rates could still be high because of the contribution of locally steep hillslope flanking incised valleys where non-linear evolution is prevailing. We propose that the observed lack of correlation between denudation and morphology is an expression of decoupling between hillslopes and channels in the lower portion of the catchments, characterized by the contrast between the steep flanks of incised valleys and the low-relief of the preserved surface.

Overall, the  $^{10}\text{Be}$ -derived denudation rates of this part of the Massif Central highlight the existence of two landscapes evolving at different rates: an equilibrated landscape, where denudation rates are correlated with the topography (river gradient and mean

catchment slope), and an out-of-equilibrium landscape characterized by a transient topography.

#### 5.4. Spatial pattern of denudation rate

We projected the  $^{10}\text{Be}$ -derived denudation rates along an east–west swath profile (Fig. 7). Where several denudation rates from the same catchment are available, subcatchment denudation rates are considered. The denudation rate distribution highlights higher values at the end and in the middle of the E–W profile and significantly lower values in the two intermediate areas in between.

This distribution is due to a combination of two effects: the large extent of the low-relief upper landscape and the projection along the swath profile of catchments located at different position. We note that the two intermediate low denudation domains correspond to the two low-relief landscapes. The first domain in the eastern portion of the profile corresponds to a region of low relief and limited river incision (Fig. 7), associated with the topographic surface around 400 m a.s.l. The second domain is developed along the west-draining (Atlantic) flank and it coincides with the low-relief topography that gently dips westward from the drainage divide from  $\sim 1200$  m a.s.l. to  $\sim 800$  m a.s.l.

At the western and eastern ends of the profile, the higher denudation rates correspond to the incised portion of the catchments where rivers cut down into the low-relief topography. The contribution of the modern landscape to the spatial pattern of the denudation rates is evident at the eastern end of the profile, where the highest three values ranging between 60 mm/kyr and 77 mm/kyr coincide with the high relief parts of the catchments.

In the middle of the profile, a high denudation rate domain with values reaching  $\sim 80$  mm/kyr is located along the drainage divide and coincides with higher elevated portions of the eastward-draining catchments. These catchments are characterized by high mean slope (up to  $15^\circ$ , vo-11), and high relief, as illustrated by the topographic swath profiles (Fig. 7), and displays equilibrated river profiles without knickpoints.

## 6. Discussion

Following the erosional landscape analysis above, we suggest that the present denudation rate and its spatial distribution in the eastern French Massif Central is controlled by two different geomorphic processes: i) westward migration of the drainage divide in the central portion of the studied area, and ii) recent rejuvenation producing an upstream moving erosive pulse in the eastern part. These two processes have been triggered by two regional uplift events.

In the following, we discuss the comparison of our data set with cosmogenic denudation data from similar regions of low tectonic activity to extract their regional significance and propose some constraints on the geodynamic evolution of the area.

### 6.1. Denudation rates in regions of low tectonic activity

Our results indicate that millennium-scale basin-averaged denudation rates in the French Massif Central are low (between 40 and 70 mm/kyr), although the region is submitted to a wet temperate climate with maximum annual precipitations of 1700 mm (from [www.meteo-mc.fr](http://www.meteo-mc.fr)). The denudation rates we determined are consistent with previous data from Schaller et al. (2001) from the northern part of the Massif Central. Overall, our results are also comparable with denudation rates found in different geodynamic contexts, such as post-orogenic mountain ranges (Matmon et al., 2003; Miller et al., 2013; Portenga and Bierman, 2011), high-relief passive margins (Mandal et al., 2015), and young orogens with low tectonic activity (i.e. Legrain et al., 2015). It is interesting to note

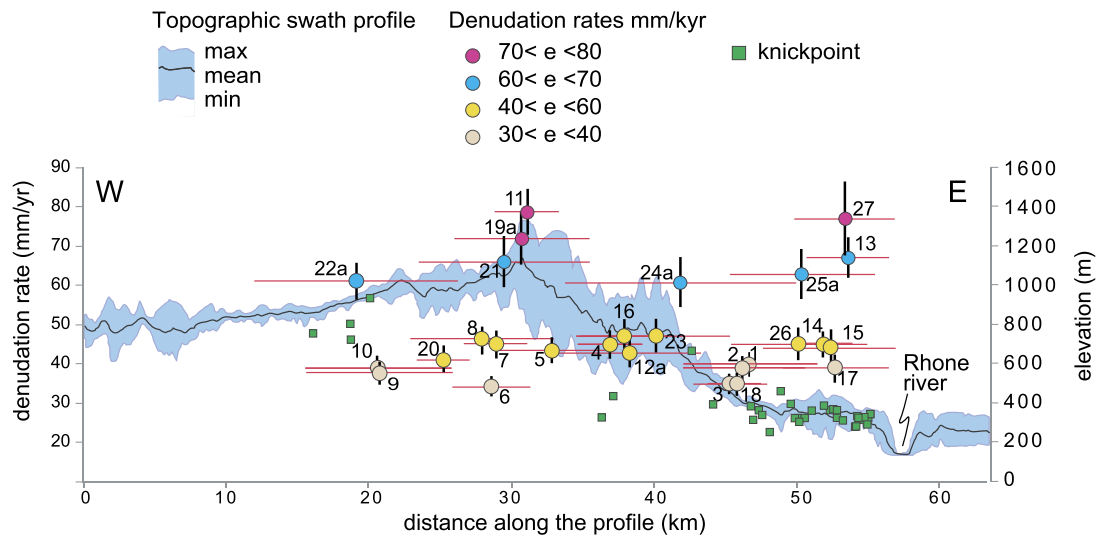


**Fig. 7.**  $^{10}\text{Be}$ -derived denudation rates projected along the east–west swath profile shown in Fig. 2. Horizontal red lines indicate the projected dimension of the catchments. Vertical lines indicates analytic uncertainties associated to the denudation rates. The spatial distribution of denudation rates shows domains of similar values: intermediate to high denudation rates are located at the extremities and in the central area while lower denudation rates are evidenced in the intermediate area characterized by lower relief. (For interpretation of the references to color in this figure legend, the reader is referred to the web version of this article.)

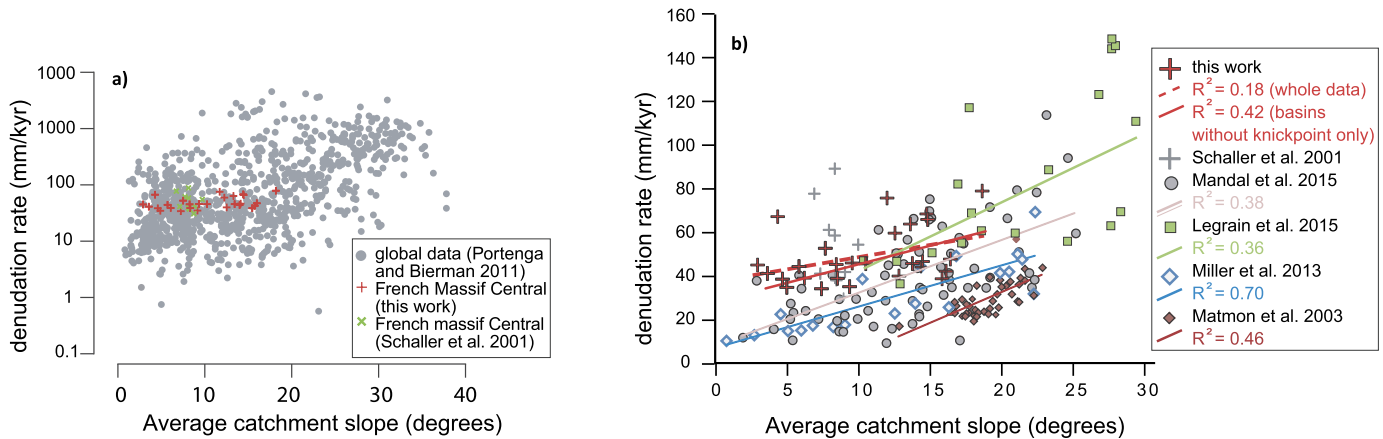


**Fig. 8.** (a) Global compilation of the relationship between  $^{10}\text{Be}$ -derived denudation rates and average catchment slope from Portenga and Bierman (2011). Red and gray crosses are data from this study and Schaller et al. (2001), respectively. (b) Relationship between denudation rate and average catchment slope for selected regions showing comparable denudation rates and slow tectonic activity.  $R^2$  correlation coefficient is shown for each region. Dotted red line is the correlation for the whole data set of this study, red line is the correlation considering the catchments without knickpoint only. (For interpretation of the references to color in this figure legend, the reader is referred to the web version of this article.)

that these denudation rates are similar, across a wide range of climatic, lithologic, topographic and geodynamic conditions.

When we compare our results from the Massif Central with a global compilation of average catchment slope and denudation rates (Portenga and Bierman, 2011), our data fall in the middle of the global distribution (Fig. 8a). The dependence of denudation rate on average slope is defined by a linear function in gentle topography and a transition to a nonlinear function when hillslope angles approach a threshold value (DiBiase et al., 2010; Ouimet et al., 2009; Ansberque et al., 2015). The Massif Central topography exhibits gentle hillslope angles and the proportion of hillslopes close to the threshold angle is limited (insert panel of Fig. 8b), as confirmed by the observed lack of landslides in the field. When compared with the global compilation, the Massif Central denudation rates show a remarkably poor sensitivity to the mean slope (Fig. 8a) and to the mean normalized steepness index.

Few cases worldwide displayed such poor sensitivity of denudation to topography, and these situations have usually been interpreted by denudation being controlled by lithological characteristics, such as bare bedrock (Granger et al., 2001) or physically

and chemically inert quartzites (Scharf et al., 2013). In our case lithological control can be ruled out and, as previously suggested, we retain that this poor correlation is due to a transient state and particularly to a decoupling between hillslope and river incision.

Many mountain ranges exhibit both transient topography and denudation rates correlated with mean slope and river steepness, demonstrating that transient state is not the primary reason of decoupling between denudation and topography, although it is sometimes invoked. For instance, in the Appalachian range (Matmon et al., 2003; Miller et al., 2013), eastern Alps (Legrain et al., 2015) and southern and northern Italy (Cyr et al., 2010), rivers exhibit transient state in response to increased uplift and denudation rates that change along the profile but are well correlated with basin mean slope and local steepness index. In these cases, enough time has passed since the last change in rock uplift or the denudation rates have been fast enough, to allow hillslope to adjust to the modification of the local base level in the rejuvenated portion of the basin. In the case of our data set, the poor correlation between denudation rate and topographic metrics is due to a strong decoupling between river incision and hillslope in the lower parts of the

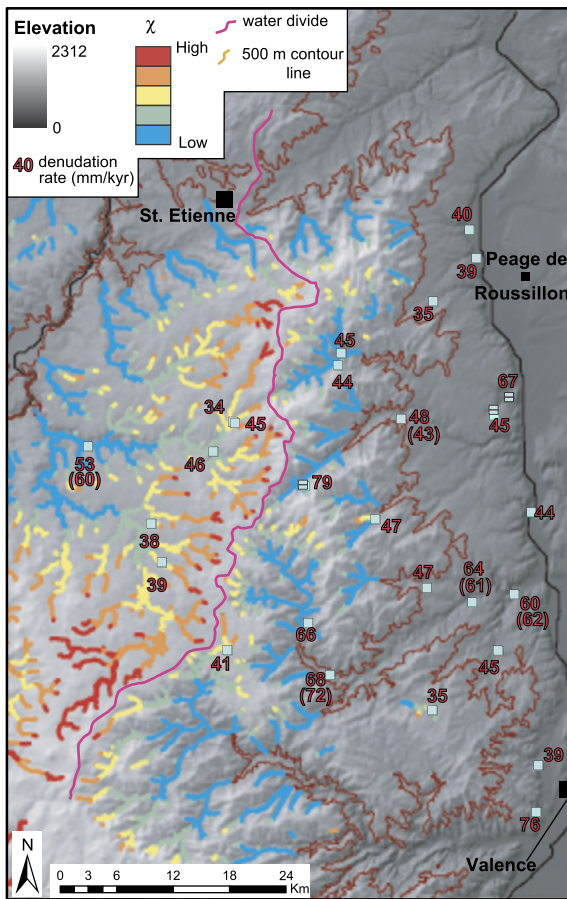


**Fig. 9.** Map of the  $\chi$  values. Higher values on the western side with respect to the eastern side suggest westward migration of the drainage divide.

catchments. Such decoupling can be enhanced by the combination of the slow hillslope evolution and rapid recent river incision.

### 6.2. Initial uplift and stream network reorganization

The spatial pattern of denudation in the central part of the studied area (Fig. 3 and Fig. 7) indicates that catchments draining the eastern side are eroding almost twice as fast as adjacent upland basins. This spatial pattern and topographic settings are found across passive continental margins (Bishop and Goldrick, 2000; Vanacker et al., 2007; Mandal et al., 2015) where the differences in denudation rates lead to migration of the drainage divide.

To investigate the river basin dynamics between eastern (Mediterranean) and western (Atlantic) draining flank, we calculated the spatial distribution of the  $\chi$  parameter (Perron and Royden, 2013; Willett et al., 2014). The parameter  $\chi$  is an integral function of the drainage area along the channel network, scaled for an arbitrary area. Differences in  $\chi$  across a drainage divide indicate a disequilibrium between adjacent catchments. Higher  $\chi$  values are associated with catchments tending to lose area with respect to the adjacent catchments with lower  $\chi$  values. In the absence of a common base level to the eastern and western catchments we calculate  $\chi$  by starting the upstream integration along the river network at 500 m a.s.l. We also note that for some rivers the integration path might include knickpoints and hence goes across stream segments with variable steepness. Despite these two caveats, the resulting map of  $\chi$  variations can still deliver first order information to support the idea of a disequilibrium across the drainage divide.

The spatial distribution of  $\chi$  across the drainage divide (Fig. 9) unambiguously shows higher values on the western flank with respect to the eastern flank, suggesting active westward migration of the drainage divide. This migration pattern and the associated difference in denudation rates are a signature of a long-wavelength morphological disequilibrium in which the main drainage divide almost coincides with the edge of the south-eastern escarpment. Processes of piracy and river captures by the west draining rivers are also evident in abrupt change of channel orientation along the drainage divide. Portions of the high-elevation low-relief surface are included in basins draining towards east, as a result of these captures.

The whole stream network seems to be currently evolving in response to asymmetric uplift. This interpretation of the topographic evolution of the Massif Central is in agreement with numerous previous authors who interpreted the eastern and southern Massif Central flank as a Mesozoic passive margin of the Tethys basin (Séranne et al., 2002; Peyaud et al., 2005). Following these interpretations, the low-relief high-elevation surface is a portion of a larger relict surface observed over the whole Massif Central. This surface results from a polyphased landscape evolution during the Mesozoic, when repeated long lasting erosion phase and gentle uplift led to the formation of thick laterites and weathering products (Fig. 9b) (Wyns and Guillocheau, 1999; Thiry et al., 1999).

The timing of the uplift of this surface is difficult to constrain. Low-temperature thermochronology data suggest that around 120 Ma the eastern margin of the massif started to exhume but probably the most important uplift phase started later. However, fission track analysis (Peyaud et al., 2005) and (U-Th)/He dating (Gautheron et al., 2009) provide cooling ages from 120 Ma to 80 Ma and 157 Ma to 38 Ma, respectively, which in term of denudation rates corresponds to mean values between 20 and 40 mm/kyr (for a geothermal gradient of  $\sim 35^\circ\text{C}/\text{km}$ ). These first order estimates are surprisingly coherent with our cosmogenic millennial-scale denudation rates suggesting that rates of erosion processes were relatively constant through time.

### 6.3. Post Miocene river incision

An additional recent rejuvenation event is needed to generate the knickpoints and the transient landscape in the lower part of the eastern flank (Fig. 10). We have shown that the low-relief surface located at elevations ranging between 300 and 400 m is perched (Fig. 5), and that paleoriver outlets are presently uplifted  $120 \pm 40$  m (minimum values) above the present base level. During the Messinian crisis, the Mediterranean sea level fell by about 1000 m (Clauzon, 1982), producing an adjustment of the Rhône river throughout the whole basin and inducing the formation of hundreds meters deep canyons (Clauzon, 1982; Loget et al., 2006). The knickpoints we observe could thus have been generated by the Messinian incision of the Rhône valley. However, we rule out this hypothesis for two reasons; first, Pliocene marine clay (Fig. S2) described by Denizot (1952) and Mandier (1988), are found today at 190 m a.s.l. (Peage de Roussillon), higher than expected for the sea level variation only (Lisiecki and Raymo, 2005), and therefore, indicate a post early Pliocene uplift. Second, after Pliocene reflooding, the knickpoints should have been below sea level and the upper river profiles should be equilibrated with the base level of the Rhône river, which reached the same elevation as before the Messinian incision. Therefore, the Messinian incision alone cannot explain the knickpoints formation, their upstream propagation and the perched surface.

Pliocene regional uplift along the middle Rhône valley was hypothesized by Denizot (1952) and Mandier (1988), who interpreted the flights of relict surfaces along the Rhône valley as Miocene in

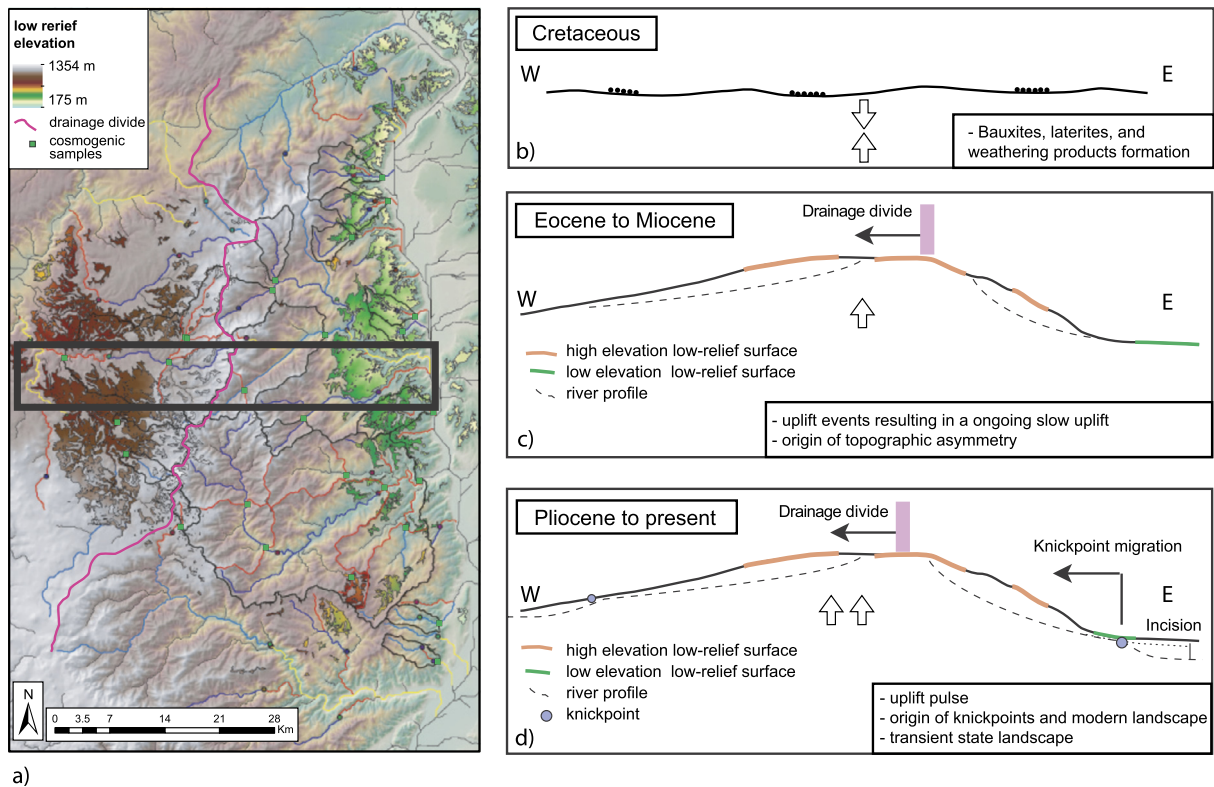


**Fig. 10.** Conceptual evolution of the Massif Central topography and present active geomorphological processes. (a) Present topographic map of the Massif Central showing the distribution and elevation of low relief surfaces. Two low relief areas are shown: the lower elevation surface at the eastern margin of the Massif Central and the higher elevation surface at the top of the margin and at the limit with the Atlantic draining area. (b) Topography inferred at the end of Cretaceous time when rock alteration produced laterites and bauxites. (c) From Cretaceous to Pliocene, the Massif Central exhibits a complex and multiphased uplift history resulting in an asymmetric topography. The drainage divide migrates westward shaping the high-standing paleo-surface. (d) An abrupt uplift event leads to a rejuvenation of the modern landscape, river incision, knickpoints formation followed by their upstream propagation.

age (known as piedmont Rhodanien). In some places, in particular in the northern part of the studied area, these surfaces are covered by thin conglomerates interpreted as Plio-Pleistocene continental deposits.

The amount of 200–300 m for the recent uplift is consistent with both present marine clays and knickpoints elevations. Moreover, this value is also consistent with the  $\sim 300$  m of post-Pliocene uplift calculated for the isostatic rebound due to unloading in the Alps due to glacial erosion starting around  $\sim 2$  Ma for the adjacent Chambaran foreland-basin (Champagnac et al., 2008). Interestingly, an increase of volcanic activity is described during the Pliocene (Michon and Merle, 2001) suggesting that a possible contribution of the mantle upwelling cannot be ruled out. At last, it is noteworthy that numerous evidences from various methods, such as palynological or geomorphological data throughout SE France (i.e. Fauquette et al., 2015 and references therein), suggest a possible post-Miocene uplift.

## 7. Conclusions

This study provides a new dataset of 27 basin-averaged denudation rates derived from  $^{10}\text{Be}$  concentrations measured in river sands from the eastern side of the French Massif Central.  $^{10}\text{Be}$ -derived denudation rates are evaluated in light of the topography and river morphometric indices to reach the following conclusions:

i) River profiles show out-of-equilibrium form. The profile of the east-draining (Mediterranean) rivers exhibit a flights of knickpoints that are coherent in elevation and generated by an erosive wave moving upstream.

ii) Denudation rates ranging from 40 to 80 mm/kyr do not show evidence for significant correlations with basin average slope, re-

lief and river morphometric parameters. The correlation improves when catchments with knickpoints are removed from the considered dataset, testifying the decoupling between hillslope and river incision beneath the knickpoint, and a transient state of the Massif Central topography.

iii) The denudation rates are regionally consistent with slight variations corresponding to different denudation domains across the eastern margin of the Massif Central. Across the drainage divide, the difference in denudation rates produce westward migration of the divide, confirmed by contrasting values of the  $\chi$  parameter.

iv) Knickpoints and transient topography are generated by a recent erosion pulse triggered by an uplift event. Prolongation of river profiles, knickpoints elevations and Pliocene marine clay elevation suggest a minimum of ca. 200 m of post-Messinian uplift.

## Acknowledgements

The authors would like to thank P. van der Beek and an anonymous reviewer for their really constructive comments and suggestions that contributed to improve the manuscript. We thank K. Manchuel for helpful discussion, M. Schaller for sharing coordinates, and F. Thomas for field support. Research and post-doctoral allocation of V.O. were funded by EDF (Electricité De France) through the SIGMA research program (Seismic Ground Motion Assessment). This work is also a contribution of the ECCOREV and Labex OT-Med (ANR-11-LABX-0061) funded by the French Government “Investissements d’Avenir” program of the French National Research Agency (ANR) through the A\*MIDEX project (ANR-11-IDEX-0001-02). The French AMS national facility ASTER (CEREGE,

Aix-en-Provence) is supported by the INSU/CNRS, ANR through the “Projets thématique d'excellence” program for the “Equipements d'Excellence” ASTER-CEREGE action, IRD and CEA.

## Appendix A. Supplementary material

Supplementary material related to this article can be found online at <http://dx.doi.org/10.1016/j.epsl.2016.03.049>.

## References

- Ahnert, F., 1970. Functional relationships between denudation, relief, and uplift in large, mid-latitude drainage basins. *Am. J. Sci.* 268 (3), 243–263.
- Ansberque, C., Godard, V., Bellier, O., De Sigoyer, J., Liu-Zeng, J., Xu, X., Ren, Z., Li, Y., ASTER Team, 2015. Denudation pattern across the Longriba fault system and implications for the geomorphological evolution of the eastern Tibetan margin. *Geomorphology* 246, 542–557.
- Balco, G., Stone, J.O., Lifton, N.A., Dunai, T.J., 2008. A complete and easily accessible means of calculating surface exposure ages or erosion rates from  $^{10}\text{Be}$  and  $^{26}\text{Al}$  measurements. *Quat. Geochronol.* 3 (3), 174–195.
- Baldwin, J.A., Whipple, K.X., Tucker, G.E., 2003. Implications of the shear stress river incision model for the timescale of postorogenic decay of topography. *J. Geophys. Res., Solid Earth* 108 (B3).
- Barruol, G., Granet, M., 2002. A Tertiary asthenospheric flow beneath the southern French Massif Central indicated by upper mantle seismic anisotropy and related to the west Mediterranean extension. *Earth Planet. Sci. Lett.* 202 (1), 31–47.
- Bishop, P., Goldrick, G., 2000. Geomorphological evolution of the East Australian continental margin. In: Summerfield, M.A. (Ed.), *Geomorphology and Global Tectonics*. John Wiley, New York, pp. 225–254.
- Blés, J.L., Bonijoly, D., Castang, C., Gras, Y., 1989. Successive post-Variscan stress fields in the French Massif Central and its borders (Western European plate): comparison with geodynamic data. *Tectonophysics* 169, 79–111.
- Champagnac, J.D., Van Der Beek, P., Diraison, G., Dauphin, S., 2008. Flexural isostatic response of the Alps to increased Quaternary erosion recorded by foreland basin remnants, SE France. *Terra Nova* 20 (3), 213–220.
- Clauzon, G., 1982. Le canyon Messinien du Rhône: une preuve décisive du “dessiccated deep-basin model” (Hsü, Cita et Ryan, 1973). *Bull. Soc. Géol. Fr.* 24 (3), 597–610.
- Cyr, A.J., Granger, D.E., Olivetti, V., Molin, P., 2010. Quantifying rock uplift rates using channel steepness and cosmogenic nuclide-determined erosion rates: examples from northern and southern Italy. *Lithosphere* 2 (3), 188–198. <http://dx.doi.org/10.1130/L96.1>.
- Denizot, G., 1952. Le Pliocène dans la vallée du Rhône. *Rev. Géogr. Lyon* 27 (4), 327–357. <http://dx.doi.org/10.3406/geoca.1952.1144>.
- Dethier, D.P., Ouimet, W., Bierman, P.R., Rood, D.H., Balco, G., 2014. Basins and bedrock: spatial variation in  $^{10}\text{Be}$  erosion rates and increasing relief in the southern Rocky Mountains, USA. *Geology* 42 (2), 167–170.
- Dewey, J.F., Helman, M.L., Knott, S.D., Turco, E., Hutton, D.H.W., 1989. Kinematics of the western Mediterranean. *Geol. Soc. (Lond.) Spec. Publ.* 45 (1), 265–283.
- DiBiase, R.A., Whipple, K.X., Heimsath, A.M., Ouimet, W.B., 2010. Landscape form and millennial erosion rates in the San Gabriel Mountains, CA. *Earth Planet. Sci. Lett.* 289, 134–144. <http://dx.doi.org/10.1016/j.epsl.2009.10.036>.
- Faccenna, C., Becker, T., Lallemand, S., Lagabriele, Y., Funicello, F., Piromallo, C., 2010. Subduction-triggered magmatic pulses: a new class of plumes? *Earth Planet. Sci. Lett.* 299 (1), 54–68. <http://dx.doi.org/10.1016/j.epsl.2010.08.012>.
- Fauquette, S., Bernet, M., Suc, J.P., Grosjean, A.S., Guillot, S., Van Der Beek, P., Jourdan, S., Popescu, S.M., Jiménez-Moreno, G., Bertini, A., Pittet, B., 2015. Quantifying the Eocene to Pleistocene topographic evolution of the southwestern Alps, France and Italy. *Earth Planet. Sci. Lett.* 412, 220–234.
- Gautheron, C.E., Tassan-Got, L., Barbarand, J., Pagel, M., 2009. Effect of alpha-damage annealing on Apatite (U–Th)/He thermochronology. *Chem. Geol.* 266, 166–179.
- Granger, D.E., Kirchner, J.W., Finkel, R., 1996. Spatially averaged long-term erosion rates measured from in situ-produced cosmogenic nuclides in alluvial sediment. *J. Geol.* 104, 249–257. <http://www.jstor.org/stable/30068190>.
- Granger, D.E., Riebe, C.S., Kirchner, J.W., Finkel, R.C., 2001. Modulation of erosion on steep granitic slopes by boulder armorings, as revealed by cosmogenic  $^{26}\text{Al}$  and  $^{10}\text{Be}$ . *Earth Planet. Sci. Lett.* 186 (2), 269–281.
- Kirby, E., Whipple, K.X., 2012. Expression of active tectonics in erosional landscapes. *J. Struct. Geol.* 44, 54–75.
- Lal, D., 1991. Cosmic ray labeling of erosion surfaces; in situ nucleide production rates and erosion models. *Earth Planet. Sci. Lett.* 104 (2–4), 424–439.
- Legrain, N., Dixon, J., Stüwe, K., von Blanckenburg, F., Kubik, P., 2015. Post-Miocene landscape rejuvenation at the eastern end of the Alps. *Lithosphere* 7 (1), 3–13.
- Lisiecki, L.E., Raymo, M.E., 2005. A Pliocene–Pleistocene stack of 57 globally distributed benthic  $\delta^{18}\text{O}$  records. *Paleoceanography* 20 (1).
- Loget, N., Davy, P., Van Den Driessche, J., 2006. Mesoscale fluvial erosion parameters deduced from modeling the Mediterranean sea level drop during the Messinian (late Miocene). *J. Geophys. Res., Earth Surf.* 111. <http://dx.doi.org/10.1029/2005JF000387>.
- Mandal, S.K., Lupker, M., Burg, J.P., Valla, P.G., Haghpor, N., Christl, M., 2015. Spatial variability of  $^{10}\text{Be}$ -derived erosion rates across the southern Peninsular Indian escarpment: a key to landscape evolution across passive margins. *Earth Planet. Sci. Lett.* 425, 154–167.
- Mandier, P., 1988. Le relief de la moyenne vallée du Rhône au Tertiaire et au Quaternaire. In: Doc. BRGM, vol. 151. 654 pp.
- Matton, A., Bierman, P., Larsen, J., Southworth, S., Pavich, M., Finkel, R., Caffee, M., 2003. Erosion of an ancient mountain range, the Great Smoky Mountains, North Carolina and Tennessee. *Am. J. Sci.* 303, 817–855. <http://dx.doi.org/10.2475/ajs.303.10.972>.
- Mazabraud, Y., Béthoux, N., Guilbert, J., Bellier, O., 2005. Evidence for short-scale stress field variations within intraplate central–western France. *Geophys. J. Int.* 160 (1), 161–178.
- Merchel, S., Arnold, M., Aumaître, G., Benedetti, L., Bourlès, D.L., Braucher, R., Al-fimov, V., Freeman, S.P.H.T., Steier, P., Wallner, A., 2008. Towards more precise  $^{10}\text{Be}$  and  $^{36}\text{Cl}$  data from measurements at the  $10^{-14}$  level: influence of sample preparation. *Nucl. Instrum. Methods Phys. Res.* 266, 4921–4926. <http://dx.doi.org/10.1016/j.nimb.2008.07.031>.
- Merle, O., Michon, L., Camus, G., de Goer, A., 1998. L'extension oligocène sur la transversale septentrionale du rift du Massif Central. *Bull. Soc. Géol. Fr.* 169 (5), 615–626.
- Meyer, H., Hetzel, R., Fügenschuh, B., Strauss, H., 2010. Determining the growth rate of topographic relief using in situ-produced  $^{10}\text{Be}$ : a case study in the Black Forest, Germany. *Earth Planet. Sci. Lett.* 290 (3–4), 391–402. <http://dx.doi.org/10.1016/j.epsl.2009.12.034>.
- Michon, L., Merle, O., 2001. The evolution of the Massif Central Rift; spatio-temporal distribution of the volcanism. *Bull. Soc. Géol. Fr.* 172 (2), 201–211.
- Miller, S.R., Sak, P.B., Kirby, E., Bierman, P.R., 2013. Neogene rejuvenation of central Appalachian topography: evidence for differential rock uplift from stream profiles and erosion rates. *Earth Planet. Sci. Lett.* 369, 1–12. <http://dx.doi.org/10.1016/j.epsl.2013.04.007>.
- Niemann, J.D., Gasparini, N.M., Tucker, G.E., Bras, R.L., 2001. A quantitative evaluation of Playfair's Law and its use in testing long-term stream erosion models. *Earth Surf. Process. Landf.* 26, 1317–1332. <http://dx.doi.org/10.1002/esp.272>.
- Nishiizumi, K., Imamura, M., Caffee, M.W., Southon, J.R., Finkel, R.C., McAninch, J., 2007. Absolute calibration of  $^{10}\text{Be}$  AMS standards. *Nucl. Instrum. Methods Phys. Res., Sect. B, Beam Interact. Mater. Atoms* 258 (2), 403–413. <http://dx.doi.org/10.1016/j.nimb.2007.01.297>.
- Ouimet, W.B., Whipple, K.X., Granger, D.E., 2009. Beyond threshold hillslopes: channel adjustment to base-level fall in tectonically active mountain ranges. *Geology* 37, 579–582. <http://dx.doi.org/10.1130/G30013A.1>.
- Perron, J.T., Royden, L., 2013. An integral approach to bedrock river profile analysis. *Earth Surf. Process. Landf.* 38 (6), 570–576.
- Peyaud, J.B., Barbarand, J., Carter, A., Pagel, M., 2005. Mid-Cretaceous uplift and erosion on the northern margin of the Ligurian Tethys deduced from thermal history reconstruction. *Int. J. Earth Sci.* 94 (3), 462–474.
- Portenga, E.W., Bierman, P.R., 2011. Understanding Earth's eroding surface with  $^{10}\text{Be}$ . *GSA Today* 21 (8), 4–10. <http://dx.doi.org/10.1130/G111A.1>.
- Schaller, M., von Blanckenburg, F., Hovius, N., Kubik, P.W., 2001. Large-scale erosion rates from in situ-produced cosmogenic nuclides in European river sediments. *Earth Planet. Sci. Lett.* 188, 441–458.
- Scharf, T.E., Codilean, A.T., De Wit, M., Jansen, J.D., Kubik, P.W., 2013. Strong rocks sustain ancient postorogenic topography in southern Africa. *Geology* 41, 331–334. <http://dx.doi.org/10.1130/G33806.1>.
- Séranne, M., Camus, H., Lucazeau, F., Barbarand, J., Quinif, Y., 2002. Surrection et érosion polyphasées de la bordure cévenole. Un exemple de morphogenèse lente. *Bull. Soc. Géol. Fr.* 173 (2), 97–112.
- Snyder, N.P., Whipple, K.X., Tucker, G.E., Merritts, D.J., 2000. Landscape response to tectonic forcing: digital elevation model analysis of stream profiles in the Mendocino triple junction region, Northern California. *Geol. Soc. Am. Bull.* 112, 1250–1263. <http://dx.doi.org/10.1130/0016-7606>.
- Stone, J.O., 2000. Air pressure and cosmogenic isotope production. *J. Geophys. Res.* 105 (B10), 23753–23759. <http://dx.doi.org/10.1029/2000JB900181>.
- Thiry, M., Simon-Coinçon, R., Schmitt, J.M., 1999. Paléoclimats kaoliniques : signification climatique et signature dans la colonne sédimentaire. *C. R. Acad. Sci. Paris, Sér. IIa* 329, 853–863.
- Tucker, G.E., van der Beek, P., 2013. A model for post-orogenic development of a mountain range and its foreland. *Basin Res.* 25 (3), 241–259.
- Vanacker, V., von Blanckenburg, F., Hewawasam, T., Kubik, P.W., 2007. Constraining landscape development of the Sri Lankan escarpment with cosmogenic nuclides in river sediment. *Earth Planet. Sci. Lett.* 253, 402–414. <http://dx.doi.org/10.1016/j.epsl.2006.11.003>.
- von Blanckenburg, F., 2005. The control mechanisms of erosion and weathering at basin scale from cosmogenic nuclides in river sediment. *Earth Planet. Sci. Lett.* 237, 462–479. <http://dx.doi.org/10.1016/j.epsl.2005.06.030>.

- Whipple, K.X., 2004. Bedrock rivers and the geomorphology of active orogens. *Annu. Rev. Earth Planet. Sci.* 32, 151–185.
- Whipple, K.X., Tucker, G.E., 1999. Dynamics of the stream-power river incision model: implications for height limits of mountain ranges, landscape response timescales, and research needs. *J. Geophys. Res.* 104 (B8), 17661–17674.
- Willett, S.D., McCoy, S.W., Perron, J.T., Goren, L., Chen, C.Y., 2014. Dynamic reorganization of river basins. *Science* 343 (6175), 1248765.
- Wobus, C., Whipple, K.X., Kirby, E., Snyder, N., Johnson, J., Spyropolou, K., Sheehan, D., 2006. Tectonics from topography: procedures, promise, and pitfalls. *Spec. Pap., Geol. Soc. Am.* 398 (303), 55–74. [http://dx.doi.org/10.1130/2006.2398\(04\)](http://dx.doi.org/10.1130/2006.2398(04)).
- Wyns, R., Guillocheau, F., 1999. Géomorphologie grande longueur d'onde, altération, érosion et bassins épicontinentaux. In: *Colloque GéoFrance 3D : résultats et perspectives*. In: *Doc. BRGM*, vol. 293, pp. 103–108.